JOURNAL OF DEGRADED AND MINING LANDS MANAGEMENT
Volume 8, Number 3 (April 2021): 2759-2768, doi:10.15243/jdmlm.2021.083.2759
ISSN: 2339-076X (p); 2502-2458 (e), www.jdmlm.ub.ac.id

Research Article

Integration of the latest Digital Terrain Model (DTM) with Synthetic Aperture Radar (SAR) Bathymetry

Atriyon Julzarika[1,2*], Trias Aditya[1], Subaryono[1], Harintaka[1], Ratna Sari Dewi[3], Luki Subehi[4]

[1] Department of Geodetic Engineering, Universitas Gadjah Mada (UGM), Jl. Grafika Bulaksumur No.2, Senolowo, Yogyakarta 55281, Indonesia
[2] Indonesian National Institute of Aeronautics and Space (LAPAN), Jl. Kalisari No. 8, Pekayon, Pasar Rebo, Jakarta 13710, Indonesia
[3] Indonesian Geospatial Information Agency (BIG), Jalan Raya Jakarta - Bogor km 46, Cibinong 16911, Indonesia
[4] Indonesian Institute of Science (LIPI), Jl. Jend. Gatot Subroto 10, Jakarta 12710, Indonesia

[*]corresponding author: verbhakov@yahoo.com

Article history:
Received 12 December 2020
Accepted 3 March 2021
Published 1 April 2021

Keywords:
DEM integration
DTM
Lake Singkarak
Rote island
SAR Bathymetry

Abstract

Topography and bathymetry integration is one of the essential things in providing height data. So far, the topography and bathymetry problems are the lack of height data availability, not up to date, and low vertical accuracy. The latest DTM is one of the topography data with up to date elevation with a spatial resolution of 5 m. Bathymetry extracted from SAR images. It is an alternative depth data for ocean bathymetry and inland water bathymetry. Topography and bathymetry integration is required to obtain comprehensive height data. This study aimed to integrate the latest DTM with SAR bathymetry. The method used in this integration was DEM integration. The method combined the latest DTM data with SAR bathymetry based on the correlation of the two data's standard deviation. The integration of the latest DTM with SAR bathymetry needs to consider differences in height reference fields. Two integration studies were conducted in this research-the latest DTM integration with ocean bathymetry for Rote Island. Then the integration of the latest DTM with inland water bathymetry in Lake Singkarak. The result of the integration is necessary to check the surface by generating longitudinal and cross-section profiles. Integrating the latest DTM and SAR bathymetry can be used for various mapping surveys on lands and waters.

To cite this article: Julzarika, A., Aditya, A., Subaryono, Harintaka, Dewi, R.S. and Subehi, L. 2021. Integration of the latest Digital Terrain Model (DTM) with Synthetic Aperture Radar (SAR) Bathymetry. Journal of Degraded and Mining Lands Management 8(3): 2759-2768, doi: 10.15243/jdmlm. 2021.083.2759.

Introduction

Geospatial information includes various basic and thematic mapping of earth resources (Hirt, 2014). A thematic map of geological resources can be generated from a detailed scale base map (Kaichang et al., 2000). Various methods and technologies are used to extract basic geospatial information, one of which is remote sensing (Bordogna et al., 2016). The development of remote sensing technology can be used for basic geospatial mapping, especially in detailed-scale 3D mapping extraction (Wilkinson, 2012). The 3D mapping includes land and waters area (Yang et al., 2017). 3D mapping for land and waters area requires height model data. This 3D mapping is needed as primary data to produce thematic geospatial information. The thematic geospatial information identifies, monitors, and land change applications in mining areas, forests, lakes, spatial planning, land dynamics, coastal, marine dynamics, and various other

thematic applications (Valeriano et al., 2004). Land dynamics caused by subsidence, uplifted, and displacement can be monitored using height model data (Gorelick et al., 2017). Likewise, the coastal dynamics monitoring in coastal environmental degradation requires height model data.

The current problem is the lack of up-to-date height models in inland areas and the lack of height model data in the waters. The height reference field difference in land and water height becomes the main problem in height mapping (Hirt, 2014). The height reference field must be equalized between the height data on land and the height data in the waters using integration data. This integration aims to make height reference for terrestrial mapping and aquatic monitoring (Gorelick et al., 2017). The height model with high vertical accuracy can be used for detailed mapping. Data integration that results in high vertical accuracy will also produce detailed thematic information on degraded and mining lands (Valeriano et al., 2004). Suppose the quality of the thematic information's accuracy and precision is better and more detailed (Aji et al., 2013). In that case, it will make it easier to carry out management related to degraded and mining lands, both on land and in waters.

In addition to the problem of differences in height reference fields, the main problem with DEM and bathymetry in Indonesia is a lack of height model data. The DEM and bathymetry are not on a detailed scale, up to date, and have high vertical accuracy (Julzarika and Harintaka, 2019). Indonesia's latest DEM data is currently DEM Nasional (DEMNAS), with acquisitions in 2010-2011 (BIG, 2019). Likewise, with the National Bathymetry (BATNAS) data, a combination of Gebco data with several bathymetry measurements in only a few areas. The available DEM and bathymetry data are not dynamic, not up-to-date, and do not represent current conditions. The latest DTM and SAR bathymetry is expected to overcome these problems. This research was proposed to integrate the latest DTM with SAR bathymetry. It will solve DEM and bathymetry problems in Indonesia. It is hoped that integrating the latest DTM and SAR bathymetry can be used for various thematic mapping of land in Indonesia.

The height model is a 3D model that includes topography and bathymetry, which describes the earth's surface (Hirt, 2014). The height model is known as DEM (Maune and Nayegandhi, 2018). Topography can be described in the form of the object surface and terrain surface (Wilson, 2012). Digital Surface Model (DSM) is a topography that describes the object's surface (Li et al., 2005). The topography that depicts the terrain's surface is called the DTM (Champion and Boldo, 2006; Zhang et al., 2016). The topography height reference area refers to the Mean Sea Level (MSL) (Hirt, 2014). There are two types of bathymetry: ocean bathymetry and inland water bathymetry (Wiehle and Pleskachevsky, 2018). The difference between these bathymetries is the location and height reference field used. Ocean bathymetry has a height reference field in the lowest water level at one tidal period (18.61 years) (IHB, 2006). Inland water bathymetry has a height reference field in the highest water level. Inland water bathymetry includes lakes, rivers, and swamps.

Topography can be extracted from terrestrial mapping and non-terrestrial mapping (Julzarika and Djurdjani, 2019). The terrestrial mapping is in the form of direct measurements in the field using a theodolite, levelling, total station, Global Navigation Satellite System (GNSS), and terrestrial Light Detection and Ranging (LiDAR) (Serrano-Juan et al., 2017; Bigdeli et al., 2018). This non-terrestrial mapping is in the form of aerial mapping, LiDAR, and remote sensing. Remote sensing data can be used for optical and SAR images (Liosis et al., 2018). The methods used to extract the DSM and DTM are stereo models, reverse stereo models, interferometry SAR (InSAR), and videogrammetry (Serrano-Juan et al., 2017; Julzarika and Djurdjani, 2019). The topography used in this paper is the latest DTM. The latest DTM describes the up to date conditions of the surface terrain. The latest DTM extraction can be done using a combination of the InSAR and Differential InSAR (DInSAR) methods. The latest DTM can be extracted using ALOS PALSAR/PALSAR-2 and Sentinel-1 images. The latest topography conditions can be extracted based on the latest displacement and adjusted to the latest Sentinel-1 image data (Costantini, 1998; Chang et al., 2019). Sentinel-1 imagery can be obtained every six days (ESA, 2013).

Bathymetry extraction can be done with terrestrial and non-terrestrial mapping (Wiehle and Lehner, 2015). The terrestrial mapping is direct measurements in waters using sonar and other bathymetry measuring instruments. The non-terrestrial mapping can be performed using aerial LiDAR; it uses the Green LiDAR sensors and Blue LiDAR sensors (Pirotti, 2010). Remote sensing data can also be used for bathymetry extraction (Mishra et al., 2014). The detail of the bathymetry information depends on the type and quality of remote sensing data used (Shen, 2018). The potential for bathymetry extraction from remote sensing data can be carried out with various data sources (Pereira et al., 2019). The bathymetry extraction includes optical data, SAR, LiDAR, altimetry, gravity, and multi-data from crowdsourced (Wiehle et al., 2019). Bathymetry extraction using optical images will provide optimal in clear waters with low turbidity and total suspended solids (TSS). The extraction is optimal at a depth of 0-25 m. SAR bathymetry extraction will result in higher vertical accuracy at normal water levels, wind speeds of 3-10 m/s, surface current velocities > 0.5 m/s, and at depths of 10-70 m (Pereira et al., 2019).

The use of LiDAR for bathymetry extraction has also proliferated (Pratomo et al., 2019). Green LiDAR sensor can extract bathymetry at a depth of 0-30 m in clear waters and has a vertical accuracy of the centimetre fraction (Allouis et al., 2015; Pratomo et al., 2019). The Blue LiDAR sensor can perform

bathymetry extraction at a depth of 25-70 cm (Allouis et al., 2015). Bathymetry extraction using altimetry satellite can extract the depth of more than 30 m (Smith and Sandwell, 1997). The use of gravity data will map the bottom topography's detailed conditions below the water surface (Brusch et al., 2011). Gravity can also be extracted using Geodesy satellite data. In addition to data sources from remote sensing, bathymetry extraction can also use crowdsourced bathymetry. It is a combination of bathymetry data from remote sensing with field measurement data. Figure 1 is a view of the multi-sources data in extracted bathymetry.

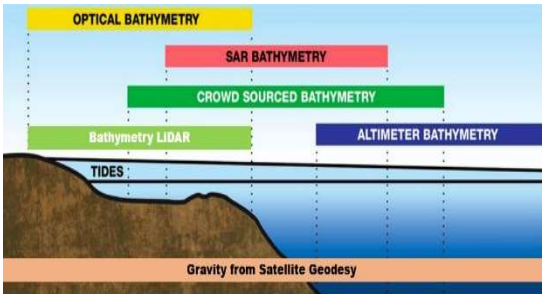

Figure 1. Combination of multi-sources data in extracted bathymetry (modified from Isardsat, 2017).

The novelty of this research is the latest DTM integration with ocean and inland water bathymetry. All of the data using SAR images and extracted using the Interferometry method. From the related literature in this study, no one has implemented the latest integration of the latest DTM with SAR bathymetry, especially in Indonesia. This study aimed to integrate the latest DTM with SAR bathymetry using the DEM integration method.

Material and Methods

In this research, topography and bathymetry integration used data from satellite images. Data for topography modelling used the latest DTM. The latest DTM was chosen because it can visualize up-to-date topographic data with high vertical accuracy. Data for ocean bathymetry and inland water bathymetry used SAR bathymetry. SAR data was chosen for bathymetry extraction because it is cloud-free, is not affected by the water turbidity effect, and data availability is free. The study area for the integration of the latest DTM with ocean bathymetry is Rote island. The study area for integrating the latest DTM with inland water bathymetry is the Semangko Fault, Lake Singkarak (Hurukawa et al., 2014).

This study chose two regions because the water area has two different height reference. The ocean area uses the lowest water level reference field, while the inland water area uses the highest water level reference field. Both of these conditions need to be studied in terms of topography integration with bathymetry. The research was carried out related to integrating the latest DTM with SAR bathymetry to solve the main problem of DEM and bathymetry availability in Indonesia. The latest DTM on Rote Island is the result of satellite image extraction in 2019. The ocean bathymetry used is 2019. The Rote area was chosen because of the completeness of the 1972-2020 period image data. The latest DTM on Lake Singkarak is the result of satellite image extraction in 2018. The inland water bathymetry used in Lake Singkarak is 2018. The Singkarak lake area was chosen because the highest water level measurement data is available for the latest DTM integration. The method in this study discussed the latest DTM, SAR bathymetry, DEM integration, surface mathematical model, and difference of height reference field. Integration of the latest DTM with SAR bathymetry can be done using the DEM integration method. This research's integration is related to; (1) the latest DTM integration with ocean bathymetry and (2) the latest DTM integration with inland water bathymetry. Both the surface integrations were tested by generating the longitudinal and cross-section profiles.

The integration carried out on Rote Island used InSAR ALOS PALSAR/PALSAR-2 and DInSAR Sentinel-1 to produce the latest DTM. Ocean bathymetry in this study used the SAR Bathymetry of equation (2). This ocean bathymetry used Sentinel-1 imagery combined with satellite altimetry and gravity data, especially at depths > 100 m. The method used to integrate the latest DTM with ocean bathymetry was by equalizing the height reference field. The depth value exceeded the MSL value was corrected based on the variance-covariance correlation value between the topography and the SAR bathymetry. This method can be done using the DEM integration equation, see equation 3. Apart from the DEM integration equation, it is also necessary to check the waterfront boundaries with multitemporal monitoring from 1972-2019. Surface shape testing on the latest DTM and SAR bathymetry can be carried out by generating longitudinal and cross-section profiles. Longitudinal profiles are used for checking areas along rivers, roads, or longitudinal surfaces.

The Semangko Fault area on Lake Singkarak was selected to integrate the latest DTM with inland water bathymetry. In this integration, the height reference area chosen is the highest water level. The latest DTM in this study used 2018 data, and SAR bathymetry uses 2018 data. The method used for integration of the topography with bathymetry was DEM integration. The integration also considers the correlation of the latest DTM data and the inland water bathymetry at the lake borderline. The correlation is variance-covariance between the latest DTM standard deviation and inland water bathymetry. This combining is adjusted to the DEM integration equation.

The latest DTM

The latest DTM is a combination of the DTM master and the latest displacement. The latest DTM is the DTM extracted from ALOS PALSAR/PALSAR-2 and

Sentinel-1, which depicts up to date conditions on the terrain surface (Julzarika and Harintaka, 2020). The up to date condition is obtained from the latest displacement extracted from Sentinel-1 using the DInSAR method (Cuevas-González et al., 2018). The reference DTM master is extracted from InSAR ALOS PALSAR/PALSAR-2 (Naidoo et al., 2016).

InSAR is a remote sensing technology that uses radar sensor images from aerial or satellite aircraft (Lusch, 1999; Ferretti et al., 2007). DInSAR is an interferometric method for detecting difference phases between at least two InSAR results (Rucci et al., 2012). This DInSAR produces vertical deformation or displacement information (Bakon et al., 2014; Dias et al., 2018). Sentinel-1 imagery can be used to extract the latest DTM every six days or extract DEM every month.

SAR Bathymetry

SAR bathymetry is a bathymetry extraction method using interferometry of a specific polarization band (Hessner et al., 1999). Each SAR image has a specific wavelength and band characteristic (Siermann et al., 2014). Four types of bands are often used in SAR bathymetry; X, C, L, and P bands (Ferretti et al., 2011). Besides, there are also several types of polarization in SAR images; HH, HV, VH, and VV (Hooper et al., 2012). SAR bathymetry can be extracted by approaching the surface roughness of seawater, lake, or river (Pereira et al., 2019) (Figure 2). Sea surface roughness dramatically determines the resulting bathymetry quality (Romeiser and Alpers, 1997; Li and Lehner, 2014).

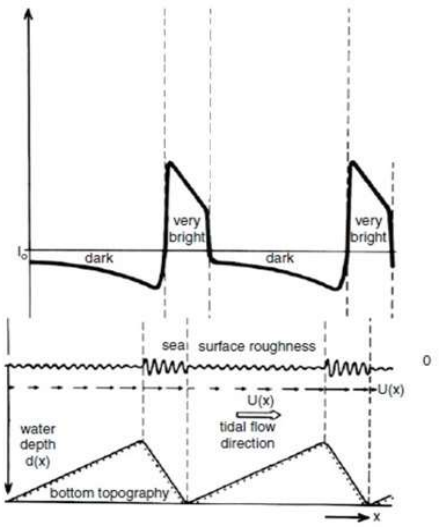

Figure 2. SAR Bathymetry using surface roughness approach (modified from Wensink and Alpers, 2015).

The type of SAR image used also determines the quality of the bathymetry extraction results (Young et al., 1985). The Sentinel-1 image used in this study is a SAR image with band C and VV polarization. The SAR bathymetry was extracted using Liqui-InSAR (LiSAR) on the surface roughness of the water surface (Wackerman et al., 1998; Pleskachevsky et al., 2011; Tarikhi, 2012). This LiSAR method has similarities with InSAR (Tarikhi, 2012) (Figure 3). There were main parameters and additional parameters used in this bathymetry extraction (Alpers and Hennings,1984; Hennings, 1989). The main parameters were phase to height and sea surface of Bragg waves.

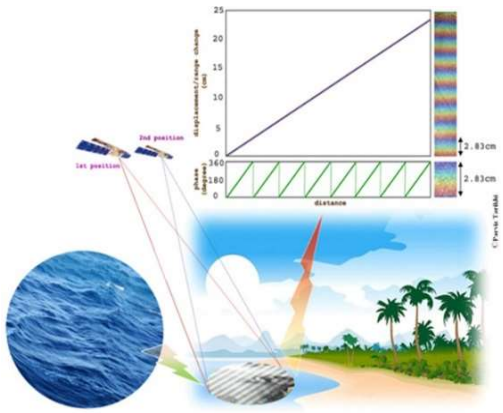

Figure 3. Liqui-InSAR (LiSAR): a method to extract the bathymetry SAR (Tarikhi, 2012).

Additional parameters used in bathymetry extraction were phase unwrapped, interferogram, backscattering of SAR images, surface currents, surface winds, surface swells, ocean gravity, hydrodynamics steepest slope, Bragg sea surface, long swell wave, sea bed geomorphology, and height wave sand (Finkl et al., 2005; Lehner et al., 2012; Pereira et al., 2019). Interferogram and phase unwrapped parameters can be substituted because they both have similar information; only the difference in visualizing the results (Costantini, 1998; Krieger et al., 2007). The interferogram is still in the reduced fringe. The phase unwrapped, there are no fringe repetitions (Costantini, 1998; Ferretti et al., 2007).

The bathymetry calculation was done by combining the formulas of Bragg, Alpers and Henning, Volterra, Brusch, and Pereira (Alpers and Rufenach, 1979; Alpers and Hennings,1984; Vogelzang, 1989; Inglada and Garello, 2002; Horstmann et al., 2015; Pereira et al., 2019). From these various methods, checking the dominant parameters using the least square adjustment approach was carried out (Mishra et al., 2014; Shen, 2018). The new algorithms used in this research were equations 1 and 2. Equation 1 is a bathymetry extraction of SAR with the main parameters. Equation 2 is a bathymetry extraction of SAR with additional parameters.

SAR Bathymetry (h_d) = Phase to height $\pm$ ((λ_0 / 2 sin θ) * (interferogram / backscattering) + (surfaces currents / surface winds)) …….. equation (1)

SAR Bathymetry (h_d) = (phase to height * Q) + (((λ_0 / 2 sin θ) * (interferogram / backscattering) * Q) +

(surface currents / surface winds) + hydrodynamics steepest slope + Bragg water surface + ocean gravity + long swell wave + height wave sand) $\pm$ e …… equation (2)

where:

λ_0 = the wavelength of SAR satellite
θ = the incidence angle
Q = co-factor matrix (1 / weight)
e = the random error

DEM integration

Combining DEM data was done using two methods; DEM integration and DEM fusion. The concept of DEM integration and DEM fusion refers to concepts developed in previous studies (Hoja and D'Angelo, 2010; Hoja et al., 2006). Some modifications were extracted, such as height error correction, height error maps generation, adding weight, detection and error removal methods (making voids), and CoKriging interpolation methods performed. Equation 3 is the DEM integration algorithm (Hoja and D'Angelo, 2010; Julzarika, 2015).

height (integration) = ((Σhi * pi) / Σpi) + void filling the gaps + delta surface fill $\pm$ e ….equation (3)

where:

hi = elevation in number pixel
pi = weighted mean height in number pixel

The best method with higher accuracy for combining DEM is integration, while the fastest method is fusion but less accuracy for combining DEM (Hoja et al., 2006; Trisakti and Julzarika, 2011). Topography and bathymetry can be combined using the DEM integration concept. The main problem that must be considered is the definition of the zero points (height reference field) on the topography of the latest DTM with the zero points in bathymetry (Vanicek and Krakiwsky, 1986).

Surface mathematical model

The extraction results of the latest DTM, SAR bathymetry, and DEM integration are influenced by the type of surface mathematical model used (Hengl and Evans, 2009). The type of order in a surface mathematical model determines whether the surface is smooth or unsmooth. A first-order polynomial will be more optimal in producing a surface similar to a field (Hengl and Evans, 2009). Areas that are hilly or mountainous will be more optimal with third-order polynomials (Kienzle, 2004). Areas with extreme elevation or depth are preferable to use fifth-order polynomials (Kienzle, 2004). In this surface modelling, the type of filter on SAR also determines DEM integration (Liu et al., 2018; Arai, 2019). Low-pass filters tend to be more suitable for lowland (Julzarika, 2015). Highland areas are more suitable for using high-pass filters (Julzarika and Djurdjani, 2019).

After surface modelling, it is necessary to reconstruct the DEM surface using Fuzzy B-Spline and Fast Fourier Transforms (FFT) (Alpers and Hennings,1984; Pereira et al., 2019). Figure 4 is a DEM reconstruction using a surface mathematical model. It aims to get a smoother surface and height error-free.

The difference of height reference field for topography and bathymetry

The reference fields of topography and bathymetry are different in height (Vanicek and Krakiwsky, 1986). Topography refers to the MSL height reference field. Bathymetry has two height reference field conditions. Ocean bathymetry refers to the lowest water level during one tidal period (18.61 years) (IHB, 2006). Inland water bathymetry refers to the highest water level. Inland water bathymetry includes lakes, rivers, and swamps.

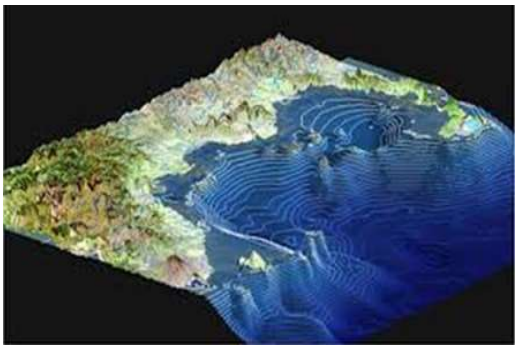

Figure 4. DEM reconstruction using a surface mathematical model.

The combination of bathymetry and topography must consider the reference height difference (Baptista et al., 2011). This combining can be done by the DEM integration method. This method considers the correlation between bathymetry and topography (Baptista et al., 2011). The correlation is in the form of variance-covariance between the standard deviation of topography and bathymetry (ASPRS, 2014). The difference between the topography and bathymetry reference field can be seen in Figure 5 (IHB, 2006).

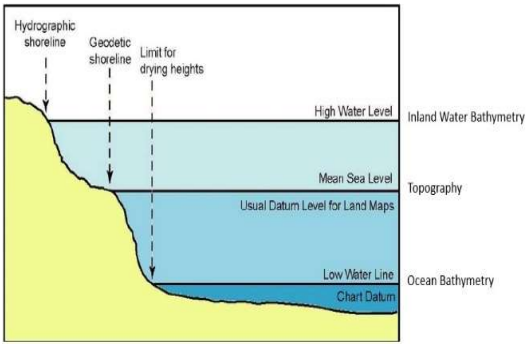

Figure 5. Height reference field of topography, ocean bathymetry, and inland water bathymetry (modified from IHB, 2006).

Results

The integration of the latest DTM with ocean bathymetry

This monitoring used satellite images and checked on coastline changes, at least one tidal period. This multitemporal monitoring used the harmonic modelling method (Julzarika et al., 2019) (Figure 6). In Figure 6. the bluish colour is water, and the bluish whiter colour is the land. The colour border area is a coastline. The principle of this harmonic method is to monitor the coastline dynamics. The coastline is changing because of the horizontal deformation. Monitoring with this harmonic becomes a cross-check of the results of DEM integration. The results of this DEM integration can be seen in Figure 7.

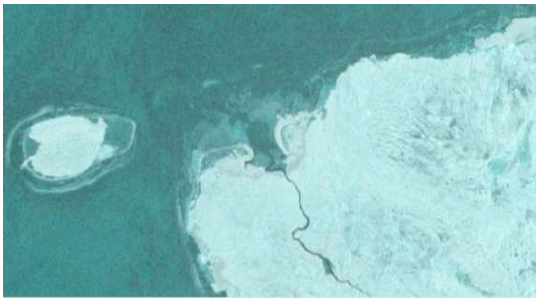

Figure 6. Coastline detection using the harmonic model method.

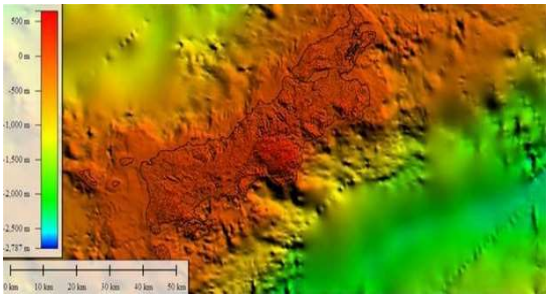

Figure 7. Integration of the latest DTM with ocean bathymetry.

Based on Figure 7, we can visually see the details of the latest SAR and DTM bathymetry. The latest DTM has a spatial resolution of 5 m, and it is capable of viewing topography details. In the SAR bathymetry, the optimal depth identified by bathymetry SAR is 10-100 m. Depths of more than 100 m can still be modelled but do not provide optimal detail so that it will have an impact on low vertical accuracy. It is recommended for depths more than 100 m to use Altimetry satellite data and gravity data from Geodesy satellites such as the combination of Grace, GOCE, and Champ data. Cross-section profiles are used for topography differences. Figure 8 is a longitudinal profile that passes through Rote Island. Figure 8 shows a longitudinal profile generated from the northern side of Rote island to the southern side. It passes through the peninsula on the western side of Rote Island. The profile view depicts a bathymetry basin at a depth of 0- (-50) m. In the peninsula, there is a smoother appearance in elevation (-1) to 1 m. This location is a topography meeting with bathymetry. The surface shape on the latest DTM integration results with ocean bathymetry is smoother because it has applied variance-covariance correlation based on the two data's standard deviation. Another check was carried out with a cross-section profile (Figure 9). Figure 9 is a cross-section profile that passes through Rote Island.

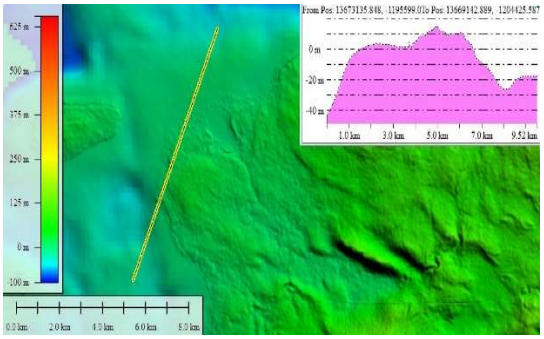

Figure 8. The longitudinal profile that passes through Rote Island.

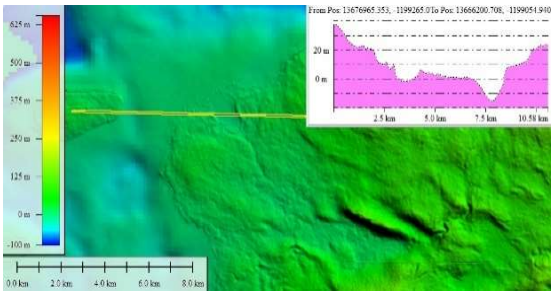

Figure 9. The cross-section profile that passes through Rote Island.

In the cross-section profile in Figure 9, we can see the shape of the bathymetry basin. The profile is generated crosswise from Rote Island to Ndao Island (left of the picture in Figure 9). The bathymetry basins represent bottom topography in the value range 0 to (-20) m. The latest DTM integration with ocean bathymetry has been seen to be smooth, especially at elevations of (-1) to 1 m.

The integration of the latest DTM with inland water bathymetry

Figure 10 is the result of the latest DTM integration with inland water bathymetry. Visually, the latest DTM integration results with inland water bathymetry are good because the height error display has not been seen. It is necessary to check the surface visualization to ensure that a height error occurs or not. It is necessary to check the surface shape after the DEM

integration is carried out. The way to do this is done by generating the longitudinal profile and a cross-section profile. The longitudinal profile follows the Semangko Fault line that extends from north to south, see Figure 10. The condition of the longitudinal profile visualizes the depth view of Lake Singkarak. The basin shape is visible at elevations < 250 m, and the basin length is about 23-25 km. The morphological depth formation of Lake Singkarak is like subsidence, cracks, and uplifted, especially from the lake edge, which is immediately steep. In addition to the longitudinal profile, a cross-section profile is generated. The cross-section profile is generated in the west to the east of Lake Singkarak (Figure 11).

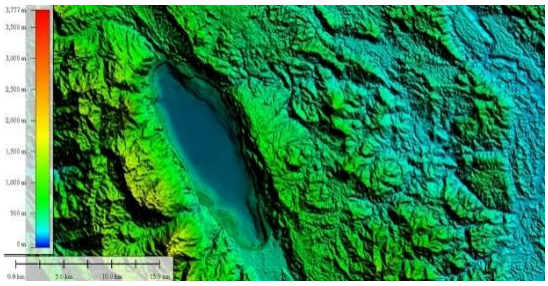

Figure 10. Integration of the latest DTM with inland water bathymetry

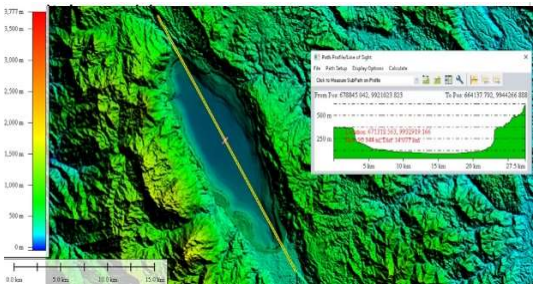

Figure 11. Longitudinal profile in Lake Singkarak.

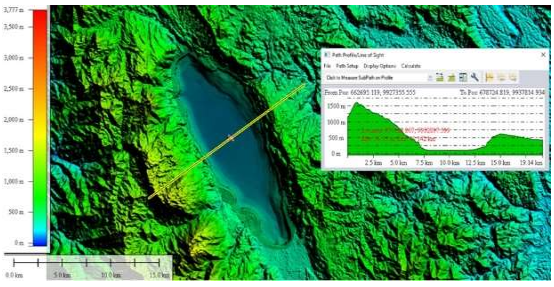

Figure 12. Cross-section profile in Lake Singkarak.

Based on the cross-section profile, the depth of Lake Singkarak from the west to the east looks like a basin. Like the longitudinal profile, the new lake basin is visible at an elevation of approximately < 250 m. On the west side, the possibility of landslides in the Lake Singkarak basin is higher than the lake's eastern side. The shape of the basin on the west side has an approaching vertical slope. Visualization of the Lake Singkarak basin can be seen in Figure 12. Based on the visualization in Figure 12, the purple colour is a basin that can fill with water. This basin is Lake Singkarak. Brownish-yellow colour is the topography of the latest DTM. The lakeside line can be identified more easily, where the purple meets brownish-yellow. The lakeside line will help calculate the lake's surface area, the lake's volume, and determine the lake borderline.

Figure 13. Visualization of the latest DTM-inland water bathymetry integration.

Discussion

The latest DTM integration results with ocean bathymetry and the latest DTM with inland water bathymetry have been obtained for the Rote and Lake Singkarak areas. The quality of the results has been carried out by generating longitudinal and cross-section profiles in both areas. According to Hoja and D'Angelo, 2010, the integration results can be checked the quality of results by comparing with field data, checking the surface profile, and conducting height difference tests. Checking the surface profile can be done by generating longitudinal and cross-section profiles. According to Trisakti & Julzarika, 2011, increasing the vertical accuracy of two height model data can improve the data's quality. The way is by integrating two height data with the consideration of the variance-covariance and standard deviation.

Another factor affecting the quality of surface-based data is the input data type in the integration. The data inputted in the form of DSM or DTM affects data integration results. Champion and Boldo, 2006 performed a robust algorithm in DSM to DTM conversion. It compared the input data of DTM to have higher vertical accuracy than DSM. The condition of changes in displacement on up to date surfaces also affects the integration data of DTM with bathymetry. It has been carried out by research of Dias et al. (2018). The ideal condition for such integration is to use a similar or adjacent image acquisition time for the latest DTM and SAR bathymetry extraction. The choice of mathematical models and digital models in integration determines the quality of vertical accuracy. According to Hengl and Evans (2009), checking surface models with longitudinal and cross-section profiles can be done for the initial vertical accuracy quality stages. It is necessary to do a height difference test and a vertical accuracy test to get more accurate and precise results. These tests are carried out by comparing against field

measurements. Further research will be carried out related to vertical accuracy testing of field measurements.

Conclusion

This paper's topic limitation is integrating the latest DTM with ocean bathymetry on Rote island and integration of the latest DTM with inland water bathymetry in Lake Singkarak. Both of these integrations use the DEM integration method. Surface shape testing is done by generating longitudinal and cross-section profiles.

There are two integration data study locations due to differences in height reference fields in ocean and inland waters. The difference in integration can be overcome by using the DEM integration method. The method combines the latest DTM data with SAR bathymetry based on the correlation of the two data's standard deviation. The integration results are that the land area has a spatial resolution of 5 m, and the ocean bathymetry more optimal in the depth of 10-100 m. Depths were more significant than 100 m can still be modelled but not optimal.

Data integration on Lake Singkarak obtained bathymetry conditions at an elevation of <250 m. Based on the longitudinal and cross-section profiles generation, the sea and lake bathymetry basins can be visualized. The basin displays several locations with cracks, uplifted, subsidence, and vertical slopes in the research location. The results of the integration of the latest DTM and SAR bathymetry are basic geospatial information that can be used for thematic geospatial information at a more detailed scale. One of the uses is for management of degraded and mining lands.

Acknowledgement

The authors wish to thank UGM, LAPAN, BIG, and LIPI, for supporting this paper's research project and writing. All authors are the main contributor to this paper.

References

Aji, A., Wang, F., Vo, H., Lee, R., Liu, Q., Zhang, X. and Saltz, J. 2013. Hadoop-GIS: A high performance spatial data warehousing system over map reduce. *Proceedings of the VLDB Endowmen* 6: 1009–1020.

Allouis, T., Bailly, J.S. and Feurer, D. 2015. *Assessing water surface effects on LiDAR bathymetry measurements in very shallow rivers: theoretical study*. UMR Territoires Environnement Télédétection et Information Spatiale (TETIS).

Alpers, W. and Hennings, I. 1984. A theory of the imaging mechanism of underwater bottom topography by real and synthetic aperture radar. *Journal of Geophysical Research: Oceans* 89: 10529-10546, doi: 10.1029/JC089iC06p10529.

Alpers, W. and Rufenach, C. 1979. The effect of orbital motions on synthetic aperture radar imagery of ocean waves. IEEE Transsactions on Antennas and Propagation 27 (5): 685-690, doi: 10.1109/TAP.1979.11421 63.

Arai, Y. 2019. Pre-treatment for preventing degradation of measurement accuracy from speckle noise in speckle interferometry. *Measurement* 136: 36-41, doi: 10.1016/j.measurement.2018.10.046.

ASPRS, 2014. *ASPRS Accuracy Standard for Digital Geospatial Data*. ASPRS. USA.

Bakon, M., Perissin, D., Lazecky, M. and Papco, J. 2014. Infrastructure Non-linear Deformation Monitoring Via Satellite Radar Interferometry. *Procedia Technology* 16: 294 - 300, doi: 10.1016/j.protcy.2014.10.095

Baptista, P., Cunha, T.R., Bernardes, C., Gama, C., Ferreira, O. and Dias, A. 2011. A precise and efficient methodology to analyze the shoreline displacement rate. *Journal of Coastal Research* 27(2): 223-232.

BIG. 2019. DEMNAS. Retrieved from http://tides.big.go.id/DEMNAS/.

Bigdeli, B., Amini Amirkolaee, H. and Pahlavani, P. 2018. DTM extraction under forest canopy using LiDAR data and a modified invasive weed optimization algorithm. *Remote Sensing of Environment* 216 (June): 289-300, doi: 10.1016/j.rse.2018.06.045.

Bordogna, G., Kliment, T., Frigerio, L., Brivio, P., Crema, A., Stroppiana, D., Boschetti, M. and Sterlacchini, S.A. 2016. Spatial data infrastructure integrating multisource heterogeneous geospatial data and time series: A study case in agriculture. *ISPRS International Journal of Geo-Information* 5(5): 73, doi: 10.3390/ijgi5050073.

Brusch, S., Held, P., Lehner, S., Rosenthal, W. and Pleskachevsky, A. 2011. Underwater bottom topography in coastal areas from TerraSAR-X data. *International Journal of Remote Sensing* 32(16): 4527-4543. doi: 10.1080/01431 161.2010.48906 3.

Champion, N. and Boldo, D. 2006. A robust algorithm for estimating digital terrain models from digital surface models in dense urban areas. *Proceedings ISPRS Commission 3 Symposium, Photogrammetric Computer Vision*.

Chang, L., Ku, O. and Hanssen, R. F. 2019. Identification of deformation pattern changes caused by enhanced oil recovery (EOR) using InSAR. *International Journal of Remote Sensing* 40(4): 1495-1505, doi: 10.1080/01431161.2018.1526426.

Costantini, M. 1998. A novel phase unwrapping method based on network programming. *IEEE Transactions on Geoscience and Remote Sensing* 36(3): 813-821, doi: 10.1109/36.673674.

Cuevas-González, M., Crosetto, M., Monserrat, O. and Crippa, B. 2018. Sentinel-1A/B imagery for terrain deformation monitoring: a strategy for Atmospheric Phase Screening (APS) estimation. *Procedia Computer Science* 138: 388-392, doi: 10.1016/j.procs.2018.10.055.

Dias, P., Catalao, J. and Marques, F.O. 2018. Sentinel-1 InSAR data applied to surface deformation in Macaronesia (Canaries and Cape Verde). *Procedia Computer Science* 138: 382-387, doi: 10.1016/j.procs.2018.10.054.

ESA, 2013. *Sentinel-1 Handbook*. European Space Agency (ESA).

Ferretti, A., Fumagalli, A., Novali, F., Prati, C., Rocca, F. and Rucci, A. 2011. A new algorithm for processing interferometric data-stacks: SqueeSAR. *IEEE Transactions on Geoscience and Remote Sensing* 49(9): 3460- 3470, doi: 10.1109/TGRS.2011.2124465.

Ferretti, A., Monti-Guarnieri, A., Prati, C. and Fabio, R. 2007. InSAR Principles: Guidelines for SAR Interferometry Processing and Interpretation.

Proceedings of the National Academy of Sciences.

Finkl, C.W., Benedet, L. and Andrews, J.L. 2005. Interpretation of seabed geomorphology based on spatial analysis of high-density airborne laser bathymetry. *Journal of Coastal Research* 21(3): 501- 514.

Gorelick, N., Hancher, M., Dixon, M., Ilyushchenko, S., Thau, D. and Moore, R. 2017. Google Earth Engine: Planetary-scale geospatial analysis for everyone. *Remote Sensing of Environment* 202: 18-27.

Hengl, T. and Evans, I.S., 2009. Mathematical and digital models of the land surface. In: Hengl, T. and Reuter, H.I. (eds.), *Geomorphometry: Concepts, Software, Applications*. Elsevier, Amsterdam, pp. 31 - 63.

Hennings, I. 1990. Radar imaging of submarine sand waves in tidal channels. *Journal of Geophysical Research* 95: 9713-9721.

Hessner, K., Reichert, K. and Rosenthal, W. 1999. Mapping of sea bottom topography in shallow water by using a nautical radar. In: *2nd International Symposium on Operationalization of Remote Sensing*, Enschede, 16–20 Aug 1999.

Hirt, C. 2014. *Encyclopedia of Geodesy*. (November), 0 – 6, doi: 10.1007/978-3-319-02370-0.

Hoja, D. and D'Angelo, P, 2010. Analysis of Dem combination methods using high resolution optical stereo imagery and interferometric SAR Data. *International Archives of the Photogrammetry, Remote Sensing and Spatial Information Science,* Volume XXXVIII, Part 1, Calgary, Canada.

Hoja, D., Reinartz, P. and Schroeder, M. 2006, Comparison of Dem generation and combination methods using high resolution optical stereo imagery and interferometric SAR Data. *International Archives of the Photogrammetry, Remote Sensing and Spatial Information Science* Volume XXXVI, Part 1, Paris, France.

Hooper, A., Bekaert, D., Spaans, K. and Arikan, M. 2012. Recent advances in SAR interferometry time series analysis for measuring crustal deformation. *Tectonophysics* 514-517: 1-13. doi: 10.1016/j.tecto.2011.10.013.

Horstmann, J., Borge, J., Seemann, J., Carrasco, R. and Lund, B., 2015. *Chapter 16 - wind, wave, and current retrieval utilizing X-band marine radars*. In: Liu, Yonggang, Kerkering, Heather, Weisberg, Robert H. (Eds.), Coastal Ocean Observing Systems. Academic Press, pp. 281–304.

Hurukawa, N., Wulandari, B.R. and Kasahara, M. 2014. Earthquake history of the Sumatran fault, Indonesia, since 1892, derived from relocation of large earthquakes. *Bulletin of the Seismological Society of America* 104(4): 1750–1762, doi: 10.1785/0120130201.

IHB, 2006. *Technical Aspect of the Law of the Sea (TALOS).* UNESCO, IOC, IHO, IAG. International Hydrographic Bureau (IHB). United Nations.

Inglada, J. and Garello, R. 2002. On rewriting the imaging mechanism of underwater bottom topography by synthetic aperture radar as a volterra series expansion. *IEEE Journal of Oceanic Engineering* 27: 665- 674, doi: 10.1109/JOE.2002.1040949.

Isardsat. 2017. *Base*. Retrieved from https://www.isardsat.space/base/.

Julzarika, A. 2015. Height model integration using Alos PALSAR, X SAR, SRTM C, and ICESAT/GLAS. *International Jornal of Remote Sensing and Earth Sciences* 12(2): 107-111 doi: 10.30536/j.ijreses.2015.v12.a2691.

Julzarika, A. and Djurdjani, D. 2019. DEM classifications: opportunities and potential of its applications. *Journal of Degraded and Mining Lands Management* 6(4): 1897-1905, doi: 10.15243/jdmlm. 2019.064.1897.

Julzarika, A. and Harintaka. 2019. Utilization of Sentinel Satellite for Vertical Deformation Monitoring in Semangko FAULT-Indonesia, (ACRS), 1–7.

Julzarika, A. and Harintaka. 2020. Indonesian DEMNAS: DSM or DTM? in 2019. *IEEE Asia-Pacific Conference on Geoscience, Electronics and Remote Sensing Technology (AGERS)* (pp. 31–36), doi: 10.1109/AGERS48446.2019.9034351.

Julzarika, A., Anggraini, N., Kayat, and Pertiwi, M. 2019. Land changes detection on Rote Island using harmonic modelling method. *Journal of Degraded and Mining Lands Management* 6(3): 1719-1725, doi: 10.15243/jdmlm. 2019.063.1719.

Kaichang, D., Deren, L. and Deyi, L. 2000. Remote sensing image classification with GIS data based on spatial data mining techniques. *Geo-spatial Information Science* 3: 30-35, doi: 10.1007/BF02829393.

Kienzle, S. 2004. The effect of DEM raster resolution on first order, second order, and compound terrain derivatives. *Transactions in GIS* 8: 83-111.

Krieger, G., Moreira, A., Fiedler, H., Hajnsek, I., Werner, M., Younis, M. and Zink, M. 2007. TanDEM-X: a satellite formation for highresolution SAR interferometry. *IEEE Transactions on Geoscience and Remote Sensing* 45(11): 3317 - 3341.

Lehner, S., Pleskachevsky, A. and Bruck, M. 2012. High-resolution satellite measurements of coastal wind field and sea state. *International Journal of Remote Sensing* 33(23): 7337-7360.

Li, X.M. and Lehner, S. 2014. Algorithm for sea surface wind retrieval from TerraSAR-X and TanDEM-X data. *IEEE Transactions on Geoscience and Remote Sensing* 52: 2928-2939, doi: 10.1109/TGRS.2013.22677 80.

Li, Z., Zhu, Q. and Gold, C. 2005. *Digital Terrain Modeling Principles and Methodology*. CRC Press. Florida. USA.

Liosis, N., Marpu, P.R., Pavlopoulos, K. and Ouarda, T.B.M.J. 2018. Ground subsidence monitoring with SAR interferometry techniques in the rural area of Al Wagan, UAE. *Remote Sensing of Environment* 216 (June): 276-288, doi: 10.1016/j.rse.2018.07.001.

Liu, Y., Zhao, C., Zhang, Q. and Yang, C. 2018. Complex surface deformation monitoring and mechanism inversion over Qingxu-Jiaocheng, China with multi-sensor SAR images. *Journal of Geodynamics* 114(January): 41- 52, doi: 10.1016/j.jog.2018.01.016.

Lusch, D.P. 1999. *Introduction to Microwave Remote Sensing.* Center for Remote Sensing. Michigan University. USA.

Maune, D.F. and Nayegandhi, A. 2018. *Digital Elevation Model Technologies and Applications: The DEM Users Manual*. American Society for Photogrammetry and Remote Sensing.

Mishra, M.K., Ganguly, D., Chauhan, P. and Ajai, 2014. Estimation of coastal bathymetry using RISAT-1 C-band microwave SAR data. *IEEE Geoscience and Remote Sensing Letters* 11(3): 671-675.

Naidoo, L., Mathieu, R., Main, R., Wessels, K. and Asner, G.P. 2016. L-band Synthetic Aperture Radar imagery performs better than optical datasets at retrieving woody fractional cover in deciduous, dry savannahs. International *Journal of Applied Earth Observation and Geoinformation* 52: 54-64, doi: 10.1016/j.jag.2016.05.006.

Pereira, P., Baptista, P., Cunha, T., Silva, P.A., Romao, S. and Lafon, V. 2019. Estimation of the nearshore bathymetry from high temporal resolution Sentinel-1A C-band SAR data - A case study. *Remote Sensing of Environment* 223: 166-178.

Pirotti, F. 2010. Assessing a template matching approach for tree height and position extraction from lidar-derived canopy height models of Pinus pinaster stands. *Forests* 1(4): 194-208, doi: 10.3390/f1040194.

Pleskachevsky, A., Lehner, S., Heege, T. and Mott, C. 2011. Synergy and fusion of optical and synthetic aperture radar satellite data for underwater topography estimation in coastal areas. *Ocean Dynamic* 61(12): 2099-2120, doi: 10.1007/s102-011-0460-1.

Pratomo, D.G., Khomsin, and Putranto, B.F.E. 2019. Analysis of the green light penetration from Airborne LiDARBathymetry in Shallow Water Area. *Geomatics International Conference 2019*. *IOP Conference Series: Earth and Environmental Science* 389 012003 IOP Publishing, doi:10.1088/1755-1315/389/1/012003.

Romeiser, R. and Alpers, W. 1997. An improved composite surface model for the radar backscattering cross section of the ocean surface: Model response to surface roughness variations and the radar imaging of underwater bottom. *Journal of Geophysical Research* 102: 25251-25267.

Rucci, A., Ferretti, A., Monti Guarnieri, A. and Rocca, F. 2012. Sentinel 1 SAR interferometry applications: The outlook for sub millimeter measurements. *Remote Sensing of Environment* 120: 156-163, doi: 10.1016/j.rse.2011.09.030.

Serrano-Juan, A., Pujades, E., Vázquez-Suñè, E., Crosetto, M. and Cuevas-González, M. 2017. Leveling vs. InSAR in urban underground construction monitoring: Pros and cons. Case of La Sagrera railway station (Barcelona, Spain). *Engineering Geology* 218: 1-11, doi: 10.1016/j.enggeo.2016.12.016.

Shen, S. 2018. Simulation study on detecting shallow bathymetry via wavelength. *IOP Conference Series Earth and Environmental Science* 170(2): 022,055.

Siermann, J., Harvey, C., Morgan, G. and Heege, T. 2014. *Satellite derived bathymetry and digital elevation models (DEM)*. *International Petroleum Technology Concerence-17346*, doi: 10.2523/IPTC-17346 –MS.

Smith, W.H.F. and Sandwell, D.T. 1997. Global sea floor topography from satellite altimetry and ship depth soundings. *Science* 277(5334): 1956-1962, doi: 10.1126/scien ce.277.5334.1956.

Tarikhi, P. 2012. Liqui-InSAR; SAR interferometry for aquatic body. *International Archives of the Photogrammetry Remote Sensing and Spatial Information Sciences* XXXIX-B7, doi: 10.5194/isprsarchives-XXXIX-B7-85-2012.

Trisakti and Julzarika, A. 2011. DEM generation from stereo ALOS Prism and its quality improvement. *International Journal of Remote Sensing and Earth Sciences* 8: 41-48.

Valeriano, D.M., Mello, E.M., Moreira, J.C., Shimabukuro, Y.E., Duarte, V. and Barbosa, C.C. 2004. Monitoring tropical forest from space: The PRODES digital project. International *Archives of the* Photogrammetry, Remote Sensing *and Spatial Information Sciences* 35: 272 – 274.

Vanicek, P. and Krakiwsky, E. 1986. *Geodesy, the Concepts*. North-Holland, Amsterdam, NY, Oxford, Tokyo.

Vogelzang J. 1989. The mapping of bottom topography with imaging radar. A comparison of the hydrodynamic modulation in some existing models. *International. Journal of Remote Sensing* 10(9): 1503-1518, doi: 10.1080/01431168908903986.

Wackerman, C., Lyzenga, D., Ericson, E. and Walker, D. 1998. Estimating near-shore bathymetry using SAR. *IGARSS 98 Symposium Proceeding* IEEE, doi: 10.1109/igars s.1998.69240 7.

Wensink, H. and Alpers, W. 2015. SAR-based bathymetry. *Ensyclopedia of Remote Sensing*. Springer, doi: 10.1007/978-0-387-36699-9_207.

Wiehle, S. and Lehner, S. 2015. Automated waterline detection in the Wadden Sea using high-resolution TerraSAR-X images. *Journal of Sensors* 2015, Article ID 450857, doi: 10.1155/2015/45085 7.

Wiehle, S. and Pleskachevsky, A. 2018. Bathymetry derived from Sentinel-1 Synthetic Aperture Radar data. In: *12th European Conference on Synthetic Aperture Radar Electronic Proceedings. Verband der Elektrotechnik Elektronik Informationstechnik e.V. Kartonhulle*, Aachen, Germany, 978-3-8007-4636-1, pp. 1489.

Wiehle, S., Pleskachevsky, A. and Gebhardt, C. 2019. Automatic bathymetry retrieval from SAR images. *CEAS Space Journal* 11: 105-114, doi: 10.1007/s12567-018-0234-4.

Wilkinson, L. 2012. *The grammar of graphics. In Handbook of Computational Statistics*. Springer: New York, NY, USA; pp. 375–414

Wilson, J.P. 2012. Digital terrain modeling. *Geomorphology* 137: 107–121.

Yang, C., Yu, M., Hu, F., Jiang, Y. and Li, Y. 2017. Utilizing cloud computing to address big geospatial data challenges. *Computer, Environment and Urban Systems* 61: 120–128.

Young, I.R., Rosenthal, W. and Ziemer, F., 1985. A three-dimensional analysis of marine radar images for the determination of ocean wave directionality and surface currents. *Journal of Geophysical Research* 90-C1: 1049-1059.

Zhang, Y., Zhang, Y., Zhang, Y. and Li, X. 2016. Automatic Extraction of DTM from Low Resolution DSM by two steps semi-global filtering. *ISPRS Annals of the Photogrammetry, Remote Sensing and Spatial Information Sciences* 3(July): 249-255, doi: 10.5194/isprs-annals-III-3-249-2016.